International Journal of Science and Research Archive
eISSN: 2582-8185
Cross Ref DOI: 10.30574/ijsra
Journal homepage: https://ijsra.net/

(RESEARCH ARTICLE)

Check for updates

Mathematical modeling and numerical study of the heat transfer process in a heat pipe

U Kh Ibragimov [1], Sh M Mirzaev [2] and OH Uzokov [2] and SS Ibragimov [2,*]

[1] *Karshi State Technical University, 180019, Khonobod st., 19, Karshi, Uzbekistan.*
[2] *Department of Heliophysics, Renewable Energy Sources and Electronics, Bukhara State University, 200117, M. Ikbol st., Bukhara, Uzbekistan.*

International Journal of Science and Research Archive, 2025, 15(01), 1446-1454

Publication history: Received on 16 March 2025; revised on 23 April 2025; accepted on 26 April 2025

Article DOI: https://doi.org/10.30574/ijsra.2025.15.1.1199

Abstract

A mathematical model has been developed and a numerical study has been conducted to determine the change in the amount of heat in a solar dryer heat pipe along its length, taking into account its geometric dimensions, outside air temperature, and solar radiation intensity. In the proposed model, the heat pipe under study is made of copper, and water is used as the working fluid. The length of the heat pipe is 0.2 m, the inner diameter is 0.045 m, and the wall thickness is 1 mm. The wick thickness is 1 mm, the porosity is 0.9, the wick conductivity is 0.0015 m2, and the effective pore radius is 54 mm. The full rate is 4.4%. The length of the evaporator and condenser is 0.05 m each. The amount of heat transferred and removed is 200 W. The operating temperature and heat flux to the heat pipe operating in steady state directly affect the steam velocity. Using the proposed model, the effect of the operating temperature on the steam dynamics was studied for four cases. The operating temperatures for these four cases are 50, 75, 100 and 120 °C. The same amount of heat is transferred in all cases. The results of modeling the change in steam velocity along the length of the pipe are presented.

Keywords: Heat pipe; Liquid; Vapor; Cell; Thermal conductivity; Thermal resistance; Viscosity

1. Introduction

Capillary forces are used to drive fluid in wick heat pipes. Heat pipes are widely used in thermal processing systems due to their high reliability and efficiency. Wick heat pipes are used for cooling electronic equipment, space devices, and thermal energy storage systems [1]. Numerous studies have been conducted to study their efficiency [2-7]. A number of different methods have been developed to improve the thermal performance and design of heat pipes. Using CFD modeling to dynamically simulate wick heat pipes is very effective. Zuo and Faghri [8] simulated heat pipes operating at a fixed thermal resistance. This model can simplify the governing equations to a first-order ordinary linear differential equation. A dynamic model of a flat plate heat pipe was developed by Huang et al. [9]. This model uses an averaged vapor phase model and solves the unstable conductivity equations for the wall and the wick. Ferrandi et al. [10] used another parameter-averaged approach which also takes into account the liquid and vapor flow. In their work, the governing equations for the liquid were solved assuming that each phase is located in two vessels (evaporator and condenser) and they are connected by a common channel. Wits and Kok [11] used a controlled volume element approach to model a small flat heat pipe. In this method, the liquid and vapor control volumes in the evaporator and condenser are separately connected to two control volumes and the governing equations are solved. Tournier and El-Genclar [12] developed a two-dimensional transient model which takes into account the energy and momentum dissipation at the liquid-vapor interface. The main focus of this research work is on the prediction of liquid accumulation. Solomon et al. [13] presented a CFD model which solved the Navier-Stokes equation for laminar and incompressible two-dimensional fluid flow. Based on the analysis of the above modeling works, a CFD model of a heat

* Corresponding author: SS Ibragimov

pipe with a wick structure was developed. The main objective of the model is to obtain information about the internal dynamics of the heat pipe based on short calculations. To achieve this goal, the two-dimensional axisymmetric geometry of the heat pipe is a large type in the axial direction for the wall, liquid and vapor. The size of the liquid bubble cells can be changed in the radial direction during the simulation. Therefore, there is no need to set fine grids at the liquid/vapor interface. Transient equations of mass, momentum and energy are solved for each cell. As a result of this approach, heat pipes can be modeled based on relatively small calculations and the internal dynamics of the pipe can be completely described. This is very useful for calculations and dynamic models of large systems with one or more heat pipes.

The geometry of the model is a two-dimensional cylindrical heat pipe using the symmetry of the pipe in the angular direction. The pipe wall, liquid and steam are the three main components of the model, each of which is modeled as a separate mass averaged in the radial direction. All of them have an arbitrary number of axial cells and do not depend on the cross-section of the heat pipe. All wall cells are subject to the same system of equations. The same applies to liquid and steam. The connection of a group of cells is shown in Figure 1.

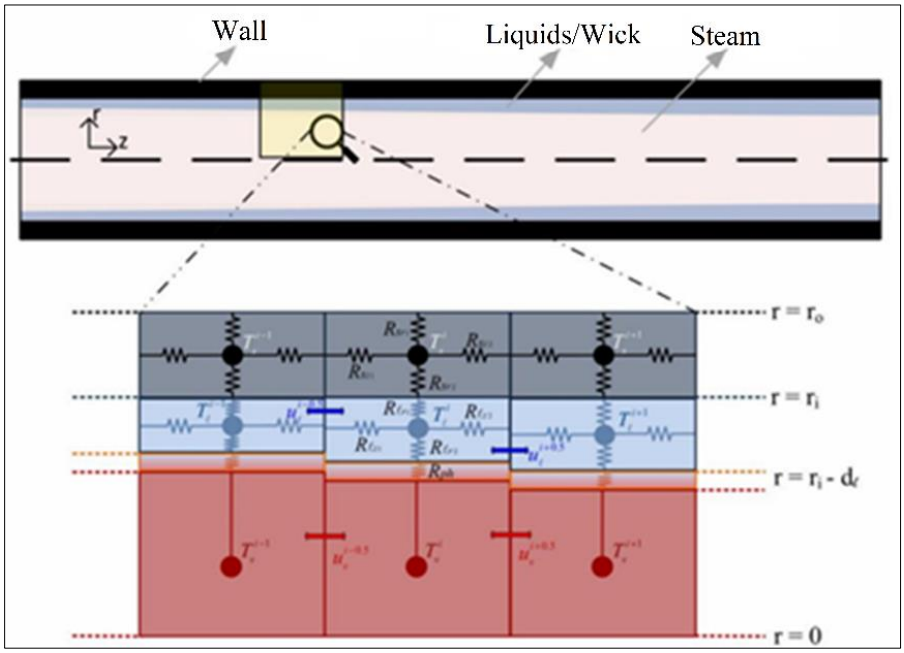

Figure 1 Model geometry and cell

Each node shown in Figure 1 above consists of a concentrated mass and characterizes the same thermodynamic state. The resistance is related to the thermal conductivity through the material and phase changes. As can be seen from the figure, the grid is staggered: the center of the cell is the temperature and pressure, and the edges are the velocity. The liquid and vapor webs can grow and shrink in the radial direction. Thus, the location of the separation boundary can be changed over time for the reading location, and the compression of the liquid can be added to the model. The architecture of the node and its connections allows the same equations to be used for the entire heat pipe.

Based on the selected geometry of the model, the following provisions were adopted during modeling:

- a symmetrical geometry axis is chosen that does not take gravity into account;
- a one-dimensional approach is used for liquid and vapor flows;
- the transferred and received heat is linearly approximated by resistance using the averaged mass [8, 14];
- the vapor is considered as an ideal gas [13, 14];
- the liquid and vapor are incompressible [14, 15];
- thermal expansion in the heat pipe container and wick is not taken into account;
- the liquid layer thickness is slightly less than the heat pipe radius [14, 16];
- the vapor dynamics are slightly higher than the dynamics of other components, so the vapor is always saturated;
- the vapor pressure drop along the heat pipe is slightly less than the liquid pressure drop [15, 16].

2. Experimental part and solutions to the problem

Based on the model geometry and assumptions, we will consider the basic equations for each component. First, the thermal resistance is defined in the radial and axial directions as follows:

$$R_{rad} = \frac{ln(\nabla_t/\nabla_i)}{2\pi k \Delta z} \quad \text{.....(1)}$$

$$R_{o\prime q} = \frac{\Delta z}{kA} \quad \text{.....(2)}$$

where R_{rad} and $R_{o\prime q}$ are the thermal resistance in the radial and axial directions, ∇_t and ∇_i are the outer and inner radii of the given resistance, k is the thermal conductivity of the part, Δz is the length of the resistance in the axial direction, A is the cross-sectional surface of the cell in the axial direction. For heat pipes with a wick structure, the effective thermal conductivity of the wick liquid is determined as follows:

$$k_{sam} = k_s \left[\frac{(k_s+k_f)-(1-\varepsilon)(k_s-k_f)}{(k_s+k_f)+(1-\varepsilon)(k_s-k_f)}\right] \quad \text{.....(3)}$$

where ε is the wick porosity, and the indices s and f denote the liquid and the wick.

Once the thermal resistance has been determined, the energy transfer equation for the wall component is given by:

$$m_d^i \frac{d\left(c_{p,d}^i T_d^i\right)}{dt} = Q + \frac{T_s^i - T_d^i}{R_{d,r2}^i + R_{s,r1}^i} + \frac{T_d^{i-1} - T_d^i}{R_{d,z2}^{i-1} + R_{d,z1}^i} + \frac{T_d^{i+1} - T_d^i}{R_{d,z2}^{i+1} + R_{d,z1}^i} \text{.....} \quad (4)$$

where c_p is the heat capacity, m is the mass of the node, T is the temperature, t is the time, Q is the amount of heat transferred to or removed from the node, d is the subscript indicating the solid wall, and i is the superscript indicating the node number. This equation expresses the relationship between the amount of energy in the wall component, the amount of external heat transferred to and removed from the node, and the thermal conductivity through the node.

The basic equations of mass, momentum and energy for the liquid component are solved simultaneously. All these equations have their own specific form in space. The continuity equation for this liquid node is expressed as:

$$\varepsilon \frac{d(\rho_s^i V_s^i)}{dt} = \varepsilon \rho_s^{i-0,5} A_s^{i-0,5} u_s^{i-0,5} - \varepsilon \rho_s^{i+0,5} A_s^{i+0,5} u_s^{i+0,5} - m_f^i \quad \text{..... (5)}$$

where ρ is the density, V is the volume, u is the velocity, m_f is the phase change velocity. The porosity is taken to be 0.6 for heat pipes with a wick structure. The Upwind scheme can be used to calculate the property at the cell boundaries.

The rate of phase change m_f and the cross-sectional area A of the fluid node are determined as follows:

$$m_f = \frac{T_s^i - T_b^i}{\left(R_{s,r2}^i + R_f^i\right)H} \text{.....} \quad (6)$$

$$A_s^i = \pi(r_{ich}^2 - (r_{ich} - d_s^i)^2) \text{.....} \quad (7)$$

where H is the latent heat, r_{ich} is the inner radius of the heat pipe, d is the thickness of the liquid layer, and b is the vapor index. The thermal resistance associated with the phase transition is often neglected because it is significantly smaller than other thermal resistances [17]. However, this thermal resistance must be taken into account when modeling a heat pipe filled with an alkali metal [18].

Liquid momentum equation:

$$\frac{d\left(\rho_s^{i+0,5} u_s^{i+0,5}\right)}{dt} = -\frac{\Delta p_s}{\Delta z\prime} - \frac{\rho_s^{i+1}\left(u_s^{i+1}\right)^2}{\Delta z\prime} + \frac{\rho_s^i (u_s^i)^2}{\Delta z\prime} + \gamma_s \quad \text{.....(8)}$$

where $\Delta z'$ is the distance between the centers of adjacent nodes, Δp is the pressure difference between adjacent nodes, and γ is the viscous component of the momentum equation. The second and third terms on the right-hand side of the

equation represent the convective components. The following equation is used to calculate the fluid velocity at the center of the cell:

$$u^i = \frac{u^{i-0,5}+u^{i+0,5}}{2} \quad \text{.....(9)}$$

The pressure coefficient for heat pipes with a wick structure is determined as follows:

$$\Delta p_s = f\frac{2\sigma}{r_k} \quad \text{.....(10)}$$

Here $\frac{2\sigma}{r_k}$ is the maximum capillary pressure [19], where σ is the surface tension, r_k is the capillary radius, and f is the correction factor that takes into account the liquid-wick contact angle between adjacent nodes [10, 11].

For laminar flows, the viscous component is calculated using the generally accepted equation:

$$\gamma_s = -\frac{\mu_s}{K}\varepsilon u_s \text{.....(11)}$$

where μ_s is the viscosity, K is the conductivity of the wick.

Calculating the viscous component for heat pipes with a wick structure is not easy. To calculate the viscous component of the liquid flow, it is necessary to know the velocity profile of the counting across the entire liquid film. However, the model only takes into account the average liquid velocity. It is known that the liquid velocity in the axial direction can be defined as a second-order polynomial in the radial coordinate [14, 20]:

$$u_s(r) = C_1 r^2 + C_2 r + C_3 \quad \text{.....} \quad (12)$$

To solve a velocity profile with three unknowns, three equations or boundary conditions are needed. The velocity profile can be solved using the following equations:

$$r = r_i \Longrightarrow u_s = 0 \text{.....(13a)}$$

$$r = r_i - d_s \Rightarrow \frac{\partial u_s}{\partial r} = 0 \quad \text{..... (13b)}$$

$$u_s = \frac{\int_0^{2\pi}\int_{r_{ich}-d_s}^{r_{ich}} u_s r dF dr}{\pi\left(r_{ich}^2-\left(r_{ich}-d_s^i\right)^2\right)} \quad \text{..... (13c)}$$

where the first equation is the viscosity boundary condition on the inner wall [21, 22], the second equation is the boundary condition taking into account the small shear stress at the liquid/vapor interface [23], and the third equation is the average velocity of the integral velocity profile along the separated liquid film in the cross-sectional area.

Only when the velocity profile is clear, the viscous component is determined by integrating the expression in equation (14) over the control volume and dividing it by the successive nodal volume:

$$\gamma = \frac{\int \mu\left(\frac{1}{r}\frac{\partial}{\partial r}\left(r\frac{\partial u}{\partial r}\right)\right)}{V} \text{.....} \quad (14)$$

The resulting expression for determining the viscous component has the form:

$$\rho_s^i V_s^i \varepsilon \frac{d\left(c_{p,s}^i T_s\right)}{dt} + \left[m_d^i \frac{d\left(c_{p,d}^i T_s^i\right)}{dt}\right] = \frac{T_d^i - T_s^i}{R_{d,r2}^i + R_{s,r1}^i} + \frac{T_b^i - T_s^i}{R_f^i + R_{s,r2}^i} +$$

$$+\left[\frac{T_s^{i-1}-T_s^i}{R_{s,z2}^{i-1}+R_{s,z1}^i} + \frac{T_s^{i+1}-T_s^i}{R_{s,z2}^{i+1}+R_{s,z1}^i}\right] \text{.....(15)}$$

The basic equations for the vapor component are the same as for the liquid component and consist of the continuity, momentum, and energy equations. The continuity equation for the vapor node is expressed as equation (16). Together

with equation (5), which defines the continuity equation for the liquid node, the total mass inside the heat pipe is also preserved:

$$\frac{d\left(\rho_b^i V_b^i\right)}{dt} = \rho_b^{i-0,5} A_b^{i-0,5} u_b^{i-0,5} - \rho_b^{i+0,5} A_b^{i+0,5} u_b^{i+0,5} + m_f^i \ldots\ldots\ldots (16)$$

Steam momentum equation:

$$\frac{d\left(\rho_b^{i+0,5} u_b^{i+0,5}\right)}{dt} = -\frac{\Delta p_b}{\Delta z\prime} - \frac{\rho_b^{i+1}\left(u_b^{i+1}\right)^2}{\Delta z\prime} + \frac{\rho_b^i\left(u_b^i\right)^2}{\Delta z\prime} + \gamma_b \ldots\ldots\ldots (17)$$

where Δp_b is the difference in vapor pressure between adjacent nodes. It is determined using the equation for calculating vapor pressure proposed by Antoine:

$$\Delta p_b = 10^{A-\frac{B}{T_b^{i+1}+C}} - 10^{A-\frac{B}{T_b^i+C}} \quad \ldots\ldots\ldots(18)$$

где A, B и C-константы уравнения Антуана.

where A, B and C are the constants of the Antoine equation.

The velocity profile throughout the steam core is expressed by a second-order polynomial:

$$u_b(r) = C_4 r^2 + C_5 r + C_6 \quad \ldots\ldots\ldots\ldots \quad (19)$$

Three equations or boundary conditions for three unknowns:

$$r = 0 \Longrightarrow \frac{\partial u_b}{\partial r} = 0 \ldots\ldots\ldots\ldots(20a)$$

$$r = r_i - d_s \Rightarrow u_b = u_s \quad \ldots\ldots\ldots(20b)$$

$$u_b = \frac{\int_0^{2\pi}\int_0^{r_{ich}-d_s} u_b r dF dr}{\pi(r_{ich}-d_s)^2} \quad \ldots\ldots\ldots\ldots(20c)$$

where the first equation represents the symmetry condition at the center of the heat pipe, the second equation represents the viscosity boundary condition at the liquid-vapor interface, and the third equation represents the average vapor velocity. Similar to the calculation of the liquid viscosity coefficient, the vapor viscosity coefficient is determined by integrating over the control volume from the expression in equation (14) and dividing it by the successive nodal volume. Therefore, the viscosity component of the vapor flow is determined using equation (21):

$$\gamma_b = \frac{\mu_b\left(4C_4(r_{ich}-d_s)^2 + 2C_5(r_{ich}-d_s)\right)}{(r_{ich}-d_s)^2} \quad \ldots\ldots\ldots\ldots (21)$$

Since the dynamics of steam are much higher than those of other components, the energy equation for steam can be calculated using the ideal gas law:

$$\frac{p_b^i}{T_b^i} = \frac{\rho_b^i R}{M} \quad \ldots\ldots\ldots\ldots \quad (22)$$

where R is the universal gas constant, M is the molecular mass of the liquid.

The boundary condition on the outer wall surface can be type II or type III:

$$r = r_0 \Longrightarrow -k\frac{dT}{dr} = Q'' \parallel -k\frac{dT}{dr} = 0 \parallel -k\frac{dT}{dr} = (h_k + h_r)[T_t - T_d] \ldots\ldots\ldots\ldots (23)$$

where r_0 is the outer radius of the heat pipe, Q is the heat flux, h_k is the convective heat transfer coefficient, h_r is the radiative heat transfer coefficient, T_t is the ambient temperature.

Boundary conditions applied to the heat pipe side cover:

$$z = 0 \wedge z = L \Longrightarrow u_s = u_b = 0 \wedge \frac{dT}{dz} = 0 \quad \ldots\ldots\ldots\ldots\ldots\ldots \quad (24)$$

where L is the length of the heat pipe.

Boundary conditions on the line of symmetry:

$$r = 0 \Longrightarrow \frac{dT}{dr} = 0 \quad \ldots\ldots\ldots\ldots\ldots\ldots \quad (25)$$

In addition, the boundary conditions given in equations (13) and (20) are used for the viscosity components.

The experimental results of Huang et al. [24] and theoretical results of Ferrandi et al. [10] were used to verify the developed dynamic models. A cylindrical copper-water heat pipe was used in their study. The outer diameter of the copper heat pipe is 19.1 mm, and the inner diameter is 17.3 mm. The length of the heat pipe is 890 mm, the length of the evaporation section is 600 mm, and a water jacket is used for convective cooling of the condenser. All other parameters used in the experiment or obtained from the experimental results (e.g., effective power, convective heat transfer coefficient in the cooling jacket) are given in the scientific paper [10].

3. Results obtained and analysis

The temperature variation in the proposed model, its comparison with the previous experiment and theoretical results, and the boundary conditions in the evaporator are shown in Figure 2. The temperatures described for the proposed model and experimental results in the research paper [24] are the average temperatures of the sections. In this case, the simulated heat pipe is divided into ten cells in the axial direction.

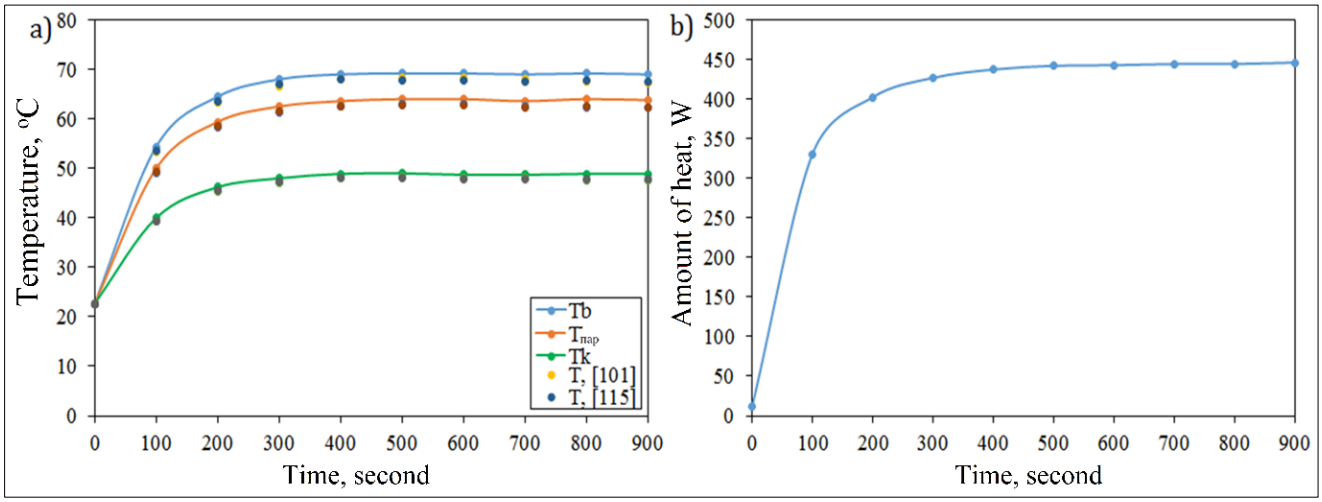

a) Comparison with Huang and Ferrandi; b) change in the amount of heat transferred from the evaporator over time

Figure 2 Transient simulation results

As can be seen from Figure 2 above, the results of the proposed model are in good agreement with the theoretical results in [10] and the experimental results in [24]. The small difference of 2.0% between the proposed model and the experimental results is due to the measurement uncertainty.

The variations in the fluid flow along the pipe height and the heat flow along the heat pipe length are shown in Figure 3. As mentioned above, very small fill factors require a very fine mesh in the axial direction. Thus, the number of meshes for the case with a small full factor is 108, and for all other cases - 36.

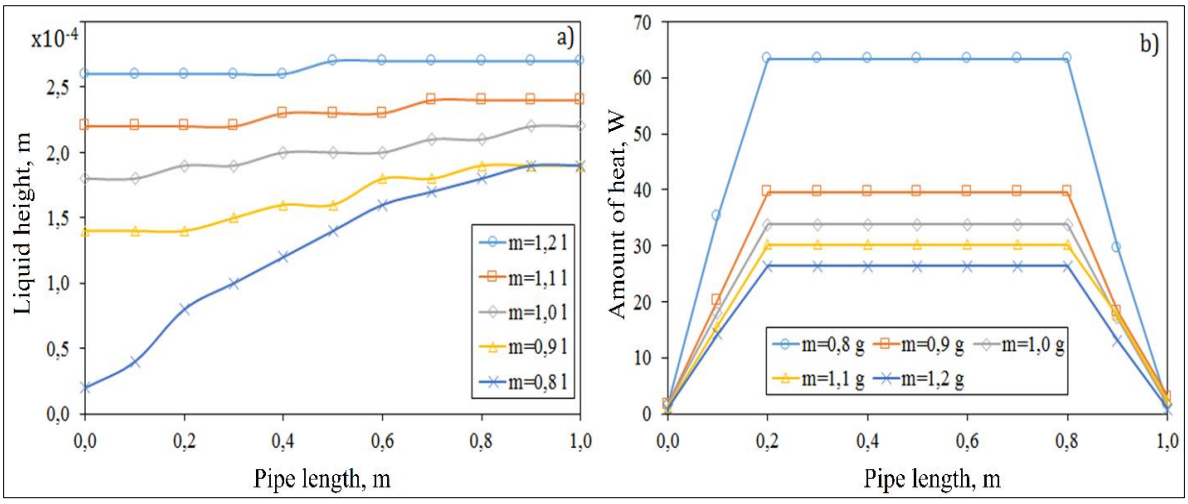

a) liquid distribution by height; b) change in heat flow by IR

Figure 3 Simulation results

From the results shown in Figure 3 above, it can be seen that 63 W of heat flux was required to obtain a difference of 10 °C between the evaporation section and the adiabatic section for the case with the lowest total efficiency, and 26 W for the case with the highest total efficiency. This is due to the high thermal resistance of the liquid component with a thick liquid film. Also, the heat exchange increased with the increase of the total efficiency in the evaporation section, and the heat exchange was carried out in the adiabatic zone. The amount of heat absorbed in the condensation zone also depends on the filling factor, and when the filling factor is high, a large amount of heat is absorbed.

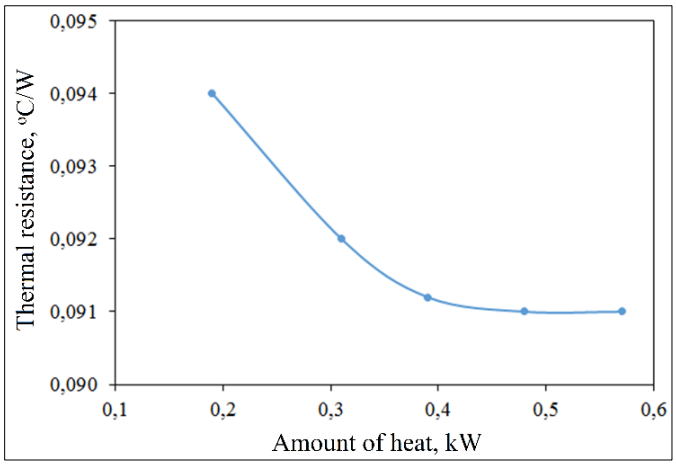

Figure 4 Results of changing the total thermal resistance in the heat pipe

The results of the total thermal resistance of the heat pipe in the proposed model are shown in Figure 4. As can be seen from the results shown in Figure 4, the thermal resistance decreased significantly with the increase of the heat flux. The change in thermal resistance is the change in the thickness of the liquid film inside the heat pipe, which in turn depends on the value of the completeness factor.

In the proposed model, the heat pipe under study is made of copper, and water is used as the working fluid. The length of the heat pipe is 0.2 m, the inner diameter is 0.045 m, the wall thickness is 1 mm. The wick thickness is 1 mm, the porosity is 0.9, the wick permeability is 0.0015 m^2, the effective pore radius is 54 mm. The full rate is 4.4%. The length of the evaporator and condenser is 0.05 m each. The amount of heat transferred and removed is 200 W.

The operating temperature and heat flux to the heat pipe operating in steady state directly affect the steam velocity. The proposed model was used to study the effect of operating temperature on steam dynamics for four cases. The operating temperatures for these four cases are 50, 75, 100, and 120 °C. The same amount of heat is transferred in all cases. The simulation results for the change in steam velocity along the pipe are shown in Fig. 5.

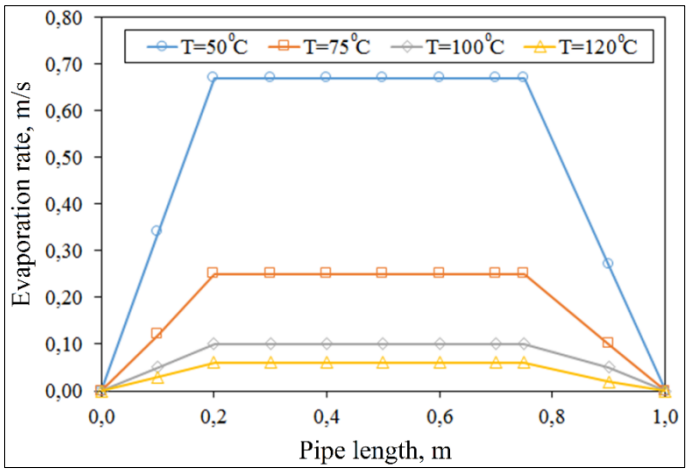

Figure 5 Results of changing the steam velocity along the length of the heat pipe at different operating temperatures

4. Conclusion

It can be seen from the results that the steam velocity increases at a low working temperature. When the steam temperature was 50°C, the steam velocity was the highest and was 0.7 m/s. This is due to the low steam density due to the low steam pressure at low temperature. At or near the sound limit, the temperature distribution along the steam channel becomes isothermal. According to the results, the steam velocity profile in the evaporator and condenser is almost linear, indicating that the temperature in the evaporator and condenser is the same. As can be seen from the results of the above theoretical studies, the results of the proposed model can be fully used in the design of copper-water heat pipes and solar dryers.

Compliance with ethical standards

Disclosure of conflict of interest

No conflict of interest to be disclosed.

References

[1] Faghri A. Review and advances in heat pipe science and technology. J. Heat Trans. 2012, 134, 123001.

[2] Kim K.S., Won M.H., Kim J.W., Back B.J. Heat pipe cooling technology for desktop PC CPU. Appl. Therm. Eng. 2003, 23. – p. 1137-1144.

[3] Lin L., Ponnappan R., Leland J. High performance miniature heat pipe. Int. J. Heat Mass Transf. 2002, 45. – p. 3131-3142.

[4] Ivanova M., Avenas Y., Schaeffer C., Dezord J.B., Schulz-Harder J. Heat pipe integrated in direct bonded copper (DBC) technology for cooling of power electronics packaging. IEEE Trans. Power Electron. 2006, 21. – p. 1541-1547.

[5] Vasiliev L.L. Micro and miniature heat pipes—Electronic component coolers. Appl. Therm. Eng. 2008, 28. – p. 266-273.

[6] Liang J., Gan Y., Li Y. Investigation on the thermal performance of a battery thermal management system using heat pipe under different ambient temperatures. Energy Convers. Manag. 2018, 155. – p. 1-9.

[7] Kuboth S., König-Haagen A., Brüggemann D. Numerical Analysis of Shell-and-Tube Type Latent Thermal Energy Storage Performance with Different Arrangements of Circular Fins. Energies 2017, 10, 274.

[8] Zuo Z.J., Faghri A. A network thermodynamic analysis of the heat pipe. Int. J. Heat Mass Transf. 1998, 41. – p. 1473-1484.

[9] Xuan Y., Hong Y., Li Q. Investigation on transient behaviors of flat plate heat pipes. Exp. Therm. Fluid Sci. 2004, 28. – p. 249-255.

[10] Ferrandi C., Iorizzo F., Mameli M., Zinna S., Mameli M. Lumped parameter model of sintered heat pipe: Transient numerical analysis and validation. Appl. Therm. Eng. 2013, 50. – p. 1280-1290.

[11] Wits W.W., Kok J.B. Modeling and validating the transient behavior of flat miniature heat pipes manufactured in multilayer printed circuit board technology. J. Heat Trans. 2011, 133, 081401.

[12] Tournier J.M., El-Genk M.S. A heat pipe transient analysis model. Int. J. Heat Mass Transf. 1994, 37. – p. 753-762.

[13] Solomon A.B., Ramachandran K., Asirvatham L.G., Pillai B.C. Numerical analysis of a screen mesh wick heat pipe with Cu/water nanofluid. Int. J. Heat Mass Transf. 2014, 75. – p. 523-533.

[14] Harley C., Faghri A. Two-dimensional rotating heat pipe analysis. J. Heat Trans. 1995, 117. – p. 202-208.

[15] Zhu N., Vafai K. Analysis of cylindrical heat pipes incorporating the effects of liquid–vapor coupling and non-Darcian transport-A closed form solution. Int. J. Heat Mass Transf. 1999, 42. –p. 3405-3418.

[16] Bertossi R., Guilhem N., Ayel V., Romestant C., Bertin Y. Modeling of heat and mass transfer in the liquid film of rotating heat pipes. Int. J. Therm. Sci. 2012, 52. – p. 40-49.

[17] Reay D., McGlen R., Kew P. Heat pipes: Theory, design and applications, 6th ed.; Butterworth-Heinemann: Oxford, UK, 2014. – p. 15-43.

[18] Hansen G., Næss E., Kristjansson K. Analysis of a vertical flat heat pipe using potassium working fluid and a wick of compressed nickel foam. Energies 2016, 9, 170.

[19] Nemec P., Caja A., Malcho M. Mathematical model for heat transfer limitations of heat pipe. Math. Comput. Model. 2013, 57. – p. 126-136.

[20] Chan S.H., Kanai Z., Yang W.T. Theory of a rotating heat pipe. J. Nucl. Energy 1971, 25. – p. 479-487.

[21] Daniels T.C., Al-Jumaily F.K. Investigations of the factors affecting the performance of a rotating heat pipe. Int. J. Heat Mass Transf. 1975, 18. – p. 961-973.

[22] Song F., Ewing D., Ching C.Y. Fluid flow and heat transfer model for high-speed rotating heat pipes. Int. J. Heat Mass Transf. 2003, 46. – p. 4393-4401.

[23] Lin L., Faghri A. Heat transfer in micro region of a rotating miniature heat pipe. Int. J. Heat Mass Transf. 1999, 42. – p. 1363-1369.

[24] Huang L., El-Genk M.S., Tournier J.M. Transient performance of an inclined water heat pipe with a screen wick. In Proceedings of the ASME 29th National Heat Transfer Conference, Atlanta, GA, USA, 8–11 August 1993.